ELEVENTH INTERNATIONAL CONFERENCE ON INTERGRANULAR AND INTERPHASE BOUNDARIES 2004

JOURNAL OF MATERIALS SCIENCE **40** (2005) 3143–3148

Interfacial thermal conductivity: Insights from atomic level simulation

SIMON R. PHILLPOT
Department of Materials Science and Engineering, University of Florida, Gainesville FL 32611, USA
E-mail: sphil@mse.ufl.edu

PATRICK K. SCHELLING
Advanced Materials Processing and Analysis Center and Department of Physics, University of Central Florida, Orlando FL 32816, USA

PAWEL KEBLINSKI
Materials Science and Engineering Department, Rensselaer Polytechnic Institute, Troy NY 12180, USA

We analyze the results of molecular-dynamics simulations of the interfacial (Kapitza) resistance of representative grain boundaries in Si. Simulations of the interactions of phonon wave packets with the Si grain boundaries show that the scattering process depends strongly on both the branch and wavelength of the incident phonons. This approach has the potential for providing detailed spectral information to mesoscale simulations of thermal transport in interfacial systems.

1. Introduction

It has long been recognized that in the presence of a heat current there is a discontinuity in temperature at an interface between two different materials [1, 2]. As a result, interfaces possess a finite thermal conductance, σ_K, known as the Kapitza conductance. The relation between the thermal current J and the temperature discontinuity at the interface ΔT is given as,

$$J = \sigma_K \Delta T \tag{1}$$

As a result of the temperature discontinuity at interfaces, a material will exhibit an effective thermal conductivity that decreases as the number of interfaces is increased. The Kapitza resistance $R_K = 1/\sigma_K$ is a measure of the resistance of an interface to the transport of heat through it. There is no general understanding of the Kapitza conductance.

In electrical insulators, the fundamental mechanism underlying the Kapitza resistance is the scattering of phonons from the interfaces. Here we describe the first steps towards developing a microscopic understanding of phonon scattering at interfaces and its relationship to thermal transport using, as described below, a judicious combination of atomic-level simulations of the interfacial conductance itself, combined with direct mechanistic simulations of phonon scattering at various kinds of interfaces.

The rest of the paper is organized as follows. In Section 2, we describe the geometry of the simulation cells used and the simulation methodologies. In Section 3, we present results for the computed Kapitza conductance for three different grain boundaries. Section 4 contains a discussion of phonon wave-packet scattering from interfaces. Section 5 contains our conclusions.

2. Simulation methods

The most direct method of computing the thermal conductivity is analogous to an experimental measurement, see Fig. 1. The simulation cell is periodic in three dimensions, with heat added in a thin slab of thickness d centered at $z = -L_z/4$ and removed from a slab of the same thickness centered at $z = +L_z/4$. When the system achieves steady state, the resulting temperature drop at the interface can be used to determine σ_K; the temperature gradient, $\mathrm{d}T/\mathrm{d}z$ in the perfect-crystal regions is a measure of the thermal conductivity of the material, k, which can be determined from Fourier's Law: $J = -\kappa\, \mathrm{d}T/\mathrm{d}z$. Although this direct method involves large temperature drops (10–100 K) and temperature gradients ($\sim 10^9$ K/m), careful simulations have established that the thermal transport coefficients can still be accurately determined [3].

The interfacial conductance is an incomplete measure of the phonon-interface interaction, since it convolutes the effects of phonons of all different branches and frequencies; moreover, it provides no mechanistic information. To dissect the mechanism of the scattering of phonons from an interface, we have developed a method of launching phonon wave packets into an interface and analyzing the subsequent scattering events.

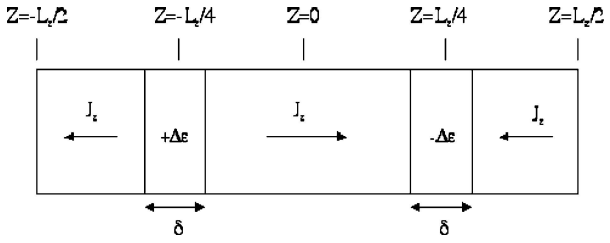

Figure 1 Schematic representation of the three-dimensional periodic simulation cell for direct computation of the Kapitza conductance. At each MD time step, energy $\Delta\varepsilon$ is added to a thin slab of atoms at $z = -L_z/4$ and is subtracted from a thin slab at $z = +L_z/4$. This results in two identical thermal currents, J_z, along the positive and negative z-axes, as labeled. The two crystallographically equivalent grain boundaries present in the cell at $z = -L_z/2$ and $z = 0$ are labeled as GB_1 and GB_2.

Phonon wave packets are formed from a linear combination of vibrational eigenstates [4].

$$u_{il\mu}(0) = \sum_{\lambda\mathbf{k}} a_{\lambda\mathbf{k}} \varepsilon_{i\mu\lambda\mathbf{k}} \exp(i\mathbf{k} \cdot \mathbf{R_1}) \qquad (3)$$

Here, $u_{il\mu}(0)$ represents the μth Cartesian component of the displacement for atom i in the unit cell labeled by l. The polarization vector, $\varepsilon_{i\mu\lambda\mathbf{k}}$, of the normal mode with wave vector $\mathbf{k}$ in band λ is determined by diagonalizing the dynamical matrix of the bulk perfect crystal. The $a_{\lambda\mathbf{k}}$, which determine the amplitude of the normal modes, are chosen to yield vibrational wave packets that are localized in both real space and wave vector space [5]. In the absence of any scattering in the system from anharmonicity or defects, the wave packets propagate without spreading or decaying. The introduction of an interface breaks the periodicity of the crystal lattice, providing a scattering site for the phonons. In principle, the interface conductance can be calculated in a straightforward manner from the full frequency and mode dependence of the transmission coefficient of phonons through the interface [4].

To gain insight into the scattering process, the atomic positions after the scattering event can be analyzed in terms of the normal modes of the bulk perfect crystal by Fourier analysis. Given the amplitude of each normal mode, it is then possible to directly compute the amount of energy contained in a given mode. By including only atoms left or right of the grain boundary, we can study the reflected and transmitted waves separately.

3. Kapitza conductance of Si grain boundaries

As a simple model system, in which to begin to develop an understanding of phonon-interface scattering we have chosen Si. The interactions are described by the Stillinger-Weber (SW) potential [6]. Fig. 2 shows the temperature profiles through three representative twist grain boundaries in Si: (001) $\theta = 43.60^\circ$ $\Sigma 29$, (001) $\theta = 11.42^\circ$ $\Sigma 101$, and (111) $\theta = 42.10^\circ$ $\Sigma 31$. The resulting temperature profiles are shown in Fig. 2 for the same thermal current in each case. It is immediately apparent that the temperature discontinuity for the (001) $\Sigma 29$ boundary is larger than that of either the (001) $\Sigma 101$ or the (111) $\Sigma 31$ boundaries. We thus

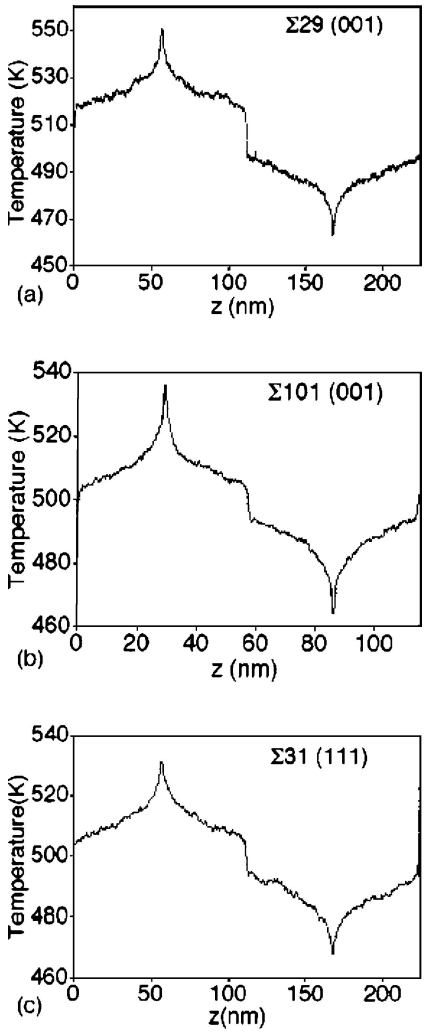

Figure 2 Temperature profiles in the presence of an applied thermal current for the (a) (001) $\theta = 43.60^\circ$ $\Sigma 29$, (b) (001) $\theta = 11.42^\circ$ $\Sigma 101$, and (c) (111) $\theta = 42.10^\circ$ $\Sigma 31$ grain-boundary systems. In each case the location of the grain boundary coincides with the discontinuous jump in the temperature profile. The applied thermal current is the same in each case.

conclude that the (001) $\Sigma 29$ boundary has the lowest Kapitza conductance; the actual values of the Kaptiza conductance are shown in Table I. Since the simulations of Maiti *et al.* [7] for two symmetric tilt GBs in Si were determined using a very similar method and also for the SW potential, they are included also. It is remarkable that, in spite of the wide variety of structures considered, and the rather different energies, the values of σ_K for the five different GBs are so very similar. While our results suggest that the amount of disorder in the grain boundary region can have a significant effect, it is apparent that σ_K for the strongly disordered (001) $\Sigma 29$ boundary is actually very close to the results of Maiti *et al.* [7] for the tilt GBs, which have a high degree of structural order. While this may suggest a difference between tilt and twist GBs, more systematic data is required before a definitive statement can be made.

4. Phonon wave-packet dynamics

While the simulations presented in the last section allowed us to make a direct comparison of σ_K for different

TABLE I Values of the Kapitza conductance for the three twist grain boundaries studied in this work at $T = 500°$K. For comparison, we also include in this table values of σ_K at 575°K taken from Maiti *et al.* [7] for two symmetric tilt grain boundaries (STGBs)

Grain boundary	E_{gb} (J/m^2)	σ_K (GW/m^{2}K) @ 500°K(*) and 575°K(†)	σ_K (GW/m^{2}K) @ 1000°K
(001) $\theta =$ 43.60° Σ29	1.32	0.80 ± 0.10*	0.99 ± 0.10
(001) $\theta =$ 11.42° Σ101	0.91	1.63 ± 0.20*	1.95 ± 0.20
(111) $\theta =$ 42.10° Σ31	0.64	1.42 ± 0.20*	1.46 ± 0.20
(310) Σ5 STGB		0.9†	–
(510) Σ13 STGB		0.8†	–

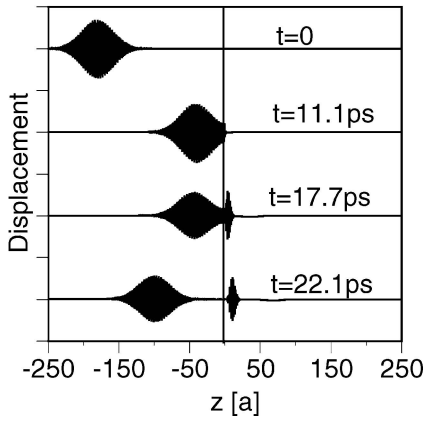

Figure 3 Snapshots of displacements for a LA wave packet with $\nu = 8.73$ THz (i.e., well above $\nu_{\max}(\text{LA} \rightarrow \text{LA}) = 6.5$ THz). Due to the difference in mass of the atoms on the two sides of the interface, the LA wave packet scatters into a LO wave-packet for $z > 0$.

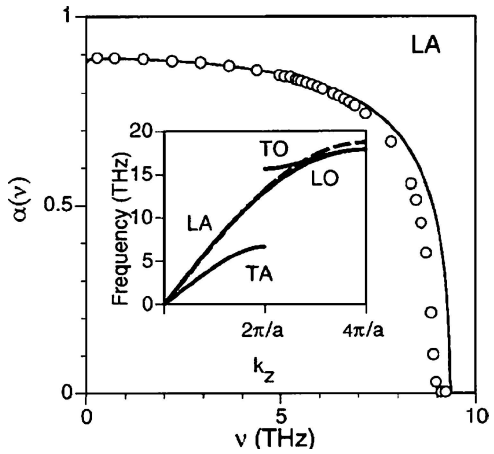

Figure 4 Frequency dependence of the energy-transmission coefficient α for incident LA wave-packets (circles). Solid line shows results from the one-dimensional spring model. The inset shows the dispersion curves for (001) phonons in Si, described by the Stillinger-Weber potential. The dotted line corresponds to the longitudinal modes of the one-dimensional spring model.

grain boundaries, they did not help us to understand the underlying scattering mechanisms. To elucidate the mechanisms of interfacial phonon scattering, before attempting to understand the GBs, we first consider a system of deceptive simplicity: an interface in which the materials on the two sides differ only by their mass. On one side of the interface the material is SW Si with the mass of Si, $M_A = 28$ amu; the material on the other side is identical, except that $M_B = 4M_A = 112$ amu. Thus there is no change in the structure at the interface itself. Because the two materials differ only in their masses, their phonon dispersion curves are identical, except that all of the frequencies in B are lower by a factor of two, and all phonon velocities are reduced by a factor of two. This sets certain limits on the available frequencies at which transmission can take place. The highest frequency longitudinal-acoustic (LA) mode in SW Si is at $\nu = 13.0$ THz. Thus, the highest frequency incident LA phonon in A that can be transmitted as an LA phonon into B is $\nu_{\max}(\text{LA} \rightarrow \text{LA}) = 13.0/2 = 6.5$ THz. Likewise the highest frequency longitudinal-optical (LO) mode in A is at 19.8 THz; thus $\nu_{\max}(\text{LA} \rightarrow \text{LO}) = 8.9$ THz. From the dispersion curves we determine $\nu_{\max}(\text{TA} \rightarrow \text{TA}) = 3.32$ THz; because of the large gap in the spectrum for the transverse phonons, conversion of transverse-acoustic (TA) phonons to transverse-optical (TO) phonons is not possible.

Using the method outlined in the previous section, we have launched phonon wavepackets from A into B. We consider first incident LA phonons. Fig. 3 shows a series of snapshots of an LA wave packet with average frequency $\nu = 8.73$ THz (i.e., well above $\nu_{\max}(\text{LA} \rightarrow \text{LA})$). We see an LA mode reflected from the interface and an LO mode transmitted with a much lower group velocity. For incident frequencies less that $\nu_{\max}(LA \rightarrow \text{LA})$, we find that both the reflected and transmitted waves have LA character.

The energy-transmission coefficient can be determined from a quantitative analysis of the data in Fig. 3. Fig. 4 shows the frequency-dependent energy-transmission coefficient for incident LA wave packets. We see a smooth decrease in α with increasing frequency. In particular, α changes continuously even at $\nu_{\max}(\text{LA} \rightarrow \text{LA})$ above which LA $\rightarrow$ LO conversion takes place. As expected from the analysis of the dispersion curves, $\alpha \rightarrow 0$ at $\nu_{\max}(\text{LA} \rightarrow \text{LO}) = 8.9$ THz.

The decrease in $\alpha(\nu)$ with increasing ν can be understood using a simple model of a one-dimensional array of masses connected by identical springs. The dashed line in the inset to Fig. 4 shows that the dispersion relation for this simple model is very similar to that of SW Si in an extended zone scheme where the LO modes may be regarded as a continuation of the LA branch. The resulting $\alpha(\nu)$ is shown for comparison in Fig. 4. The level of agreement is remarkably high, reflecting the similarity of the dispersion relations shown in the inset.

Phonons in the TA branch are more complicated than phonons in the LA branch because the polarization direction has to be taken into account. To vary the polarization of the incident wave packet, at each k-vector we form different linear combinations of the two degenerate TA modes. We find that the value of α varies with the polarization of the incident wave in a systematic manner, with the effect of polarization becoming more pronounced with increasing frequency [8].

The results on this artificially simple interface can be understood purely in terms of the properties of the

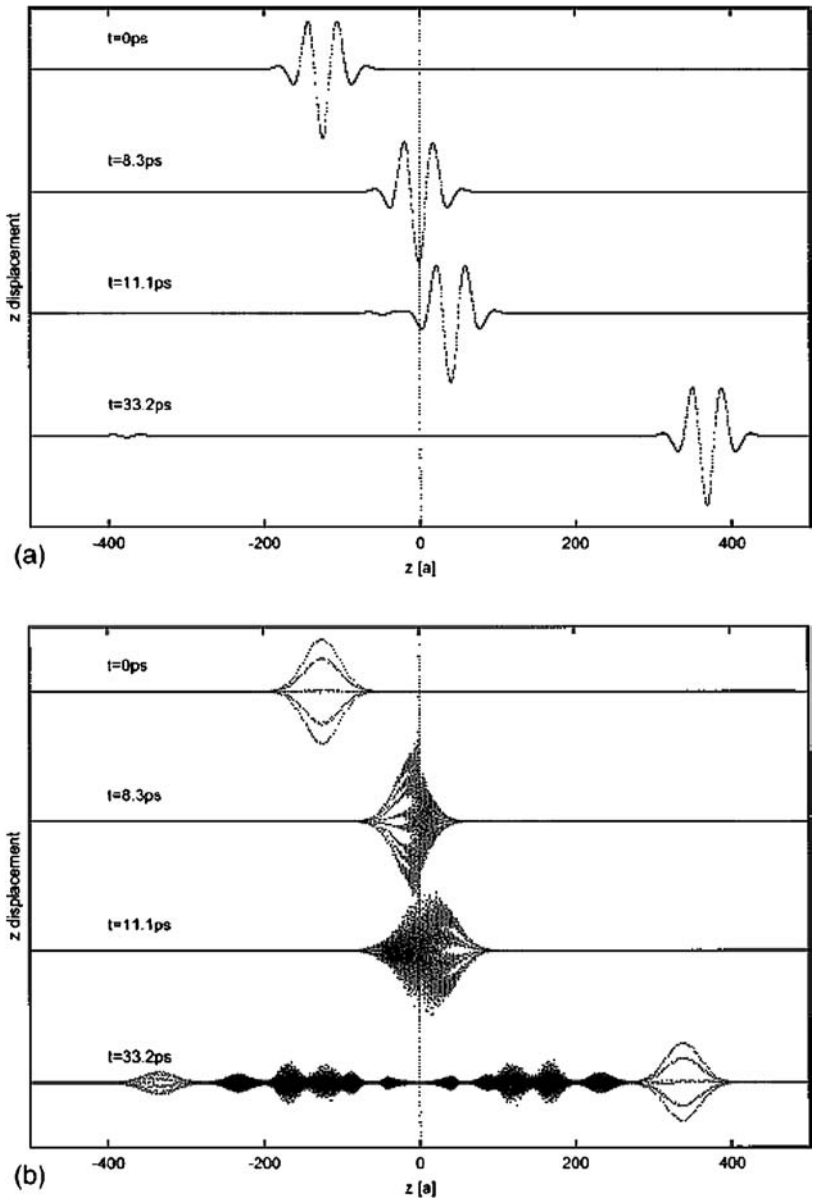

Figure 5 Snapshots of the z displacement of atoms for the case of an LA wave-packet scattering from the (001) Σ29 grain boundary: (a) $k_z \sim 0.025(2\pi/a_0)$, and (b) $k_z \sim 0.400(2\pi/a_0)$. The vertical dotted line at $z = 50$ indicates the location of the grain boundary.

materials on the two sides. However, real grain boundaries have complicated structures, with local atomic environments very different from the bulk. Moreover, for the symmetric twist boundaries we consider here, the GB normal is the same on the two sides of the interface. Thus for LA and LO modes, the vibrational properties on the two sides of the interface are identical; for TA and TO modes, there is a difference on the two sides, arising from the twist rotation.

We have investigated the scattering of phonon wave packets from two of the GBs investigated above, namely the (001) Σ29 and the (001) Σ101. We focus on LA modes because they are the most important branch for thermal transport. In particular, we consider the case where the incident wave packet has a wave vector perpendicular to the interface. In other words, the wave vector of the incident phonon is parallel to the z-axis: $k_z \neq 0$, whereas $k_x = 0$ and $k_y = 0$.

In Fig. 5a and b we show snapshots at different times of the z-displacement of the atoms as a function of position along the z direction in the simulation cell from the (001) Σ29 GB for two different incident wave vectors. Fig. 5a shows the scattering of a phonon wave packet with a very long average wavelength of $40a_0$, corresponding to an average frequency of 0.37 THz and a wave vector of $k_z = 0.025(2\pi/a_0)$. It is apparent that this wave packet is almost unaffected by the presence of the grain boundary, and nearly all the incident energy is transmitted to the region $z > 0$. By contrast, the wave packet shown in Fig. 5b, with an average wavelength of $2.5a_0$ and frequency and wave vector of 5.81 THz and $k_z = 0.400(2\pi/a_0)$, is strongly scattered by the interface, with a significant amount of the total energy being reflected back to the region $z < 0$. The spread in real space of the atomic displacements seen in Fig. 5b at 33.2 ps suggests that a significant amount of the incident energy has been scattered into modes different from the incident wave packet. We saw no such effects in the phonon scattering from the simple interfaces in Fig. 3.

Fig. 6 shows the frequency dependence of the transmission coefficient α of wave packets comprised of

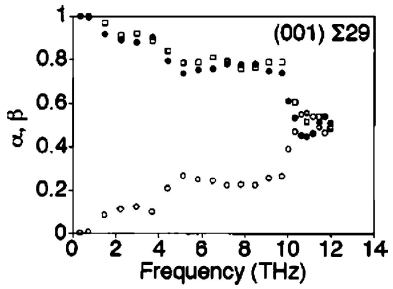

Figure 6 Frequency dependence of the energy transmission coefficient, α (filled circles), and reflection coefficient, β (open circles), for incident LA wave packets scattered from the (001) Σ29 GB in Si. Since all energy is either reflected from or transmitted through the boundary, $\alpha + \beta = 1$. The squares denote α for a simulation cell containing 2×2 cells of the (001) Σ29 grain boundary system.

LA modes scattering from the (001) Σ29 grain boundary, compiled from an analysis of snapshots such as those at the latest time in Fig. 5a and b. Also shown in Fig. 6 is the reflection coefficient β, which is defined to be the fraction of the incident energy that is reflected from the grain boundary to the region $z < 0$. Since all of the incident energy is either transmitted to the region $z > 0$ or reflected to the region $z < 0$, $\alpha + \beta = 1$ for each incident frequency. The squares in Fig. 6 correspond to a simulation cell is twice as large in the x-y dimensions (i.e. 4 times the area), demonstrating that size effects in the x-y plane are unimportant.

To analyze the phonon scattering in detail, we have performed Fourier analyses of the reflected and transmitted waves. To characterize the component of the wave vector parallel to the interface, it is useful define a quantity $k_{xy} = \sqrt{k_x^2 + k_y^2}$. In Fig. 7, the transmitted wave from Fig. 5b into three components: an unscattered LA mode, i.e., a mode with the same k-vector as the incident wave packet, for which $k_{xy} = 0$; a scattered LA mode which has $k_{xy} \neq 0$; and TA modes. Since, none of the incident LA modes has sufficient energy to create optical modes, they need not be considered here. Much of the incident wave packet is not scattered and remains in LA modes with $k_{xy} = 0$. This unscattered wave packet is closely followed by wave packets comprised of LA modes with $k_{xy} \neq 0$. Finally, a significant amount of energy is found in TA modes. The relative positions of the wave packets can be understood in terms of the z-component of the group velocities of the different modes. Although there is a significant amount of mode conversion, we find that only modes with vibrational frequencies equal to the frequency of the incident wave packet are excited. Thus these interactions are completely elastic.

The results presented here for the scattering of boundaries show for the first time in detail the mechanism of phonon scattering from grain boundaries. Consistent with our expectations from the MD simulations of the Kaptiza conductance presented in Section 3, the (001) Σ29 boundary scatters phonons more strongly than the lower energy (001) Σ101 boundary. In both cases, in the limit of very low frequency, the wave packet passed through the grain boundary with essentially no scattering. By contrast, as the frequency of the incident wave packet is increased, significant mode conversion takes place.

5. Outlook

Our theoretical understanding of phonon-mediated interfacial thermal transport is still in its infancy.

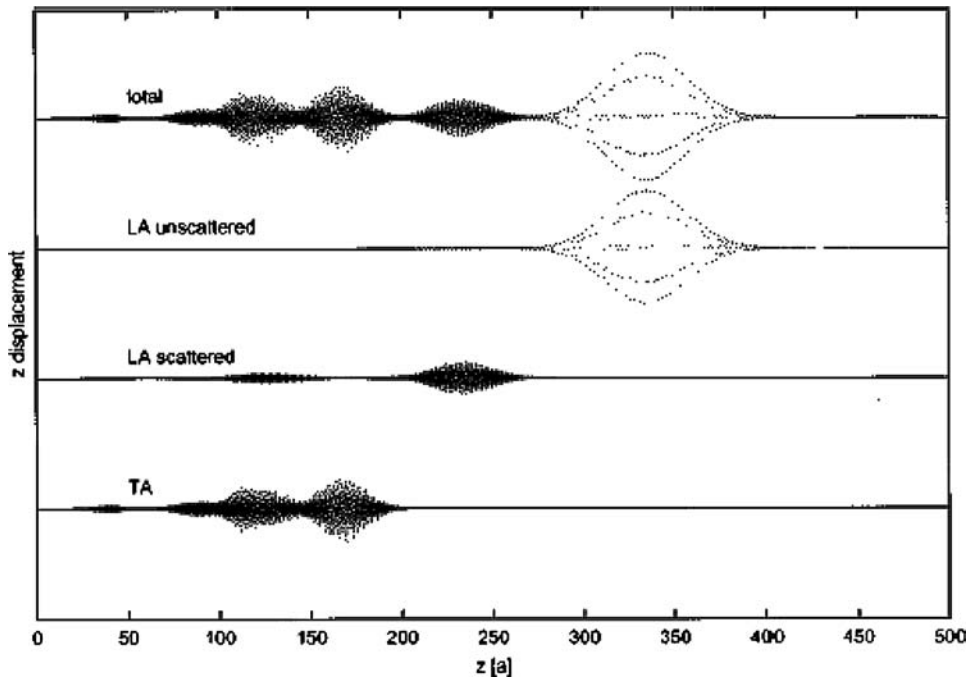

Figure 7 Analysis of the transmitted wave packets for a wave packet with $k_z = 0.40(2\pi/a_0)$ incident on the (001) Σ29 GB. The displacements in this picture correspond to those in Fig. 5b at $t \sim 33.2$ ps. The top panel shows the total atomic displacements. The second panel shows only the components of the wave that correspond to LA modes with $k_{xy} = 0$. Because these modes are the same as those that comprised the incident wave packet, this part of the transmitted wave is unscattered. The third panel shows the scattered LA modes i.e., those modes that have $k_{xy} \neq 0$. Finally, he bottom panel shows the displacements that are just due to TA modes.

However, many of the simulation tools required to develop this understanding now exist. Although not discussed above, there is a direct and rigorous formalism by which the phonon transmission coefficients can be used to determine the thermal conductivity. However, this requires knowledge of the transmission coefficient for all modes and frequencies, information that is not yet available for even a single (model) grain boundary.

There are two traditional theoretical approaches to understanding interfacial thermal transport. In the acoustic mismatch model (AMM), the transmission coefficient is determined from the differing acoustic impedances—the product of the sound speed and density—on the two sides of the interface. In the diffuse mismatch model (DMM), it is assumed that all phonons are absorbed by the boundary and re-emitted in direct proportion to the phonon density of states on each side. It is noteworthy that neither approach takes into account the structure or properties of the interface itself. It is instructive to compare our results to the predictions of the AMM and DMM. Since the AMM deal only with the mass density and elastic constants, it predicts that the grain boundaries studied here should completely transmit all the incident energy, i.e., $\alpha = 1$, which is indeed the case for $\omega \rightarrow 0$ (see Figs 3 and 6). However, as the frequency of the incident wave packet increases, the energy-transmission coefficient becomes significantly less than unity. For a very disordered interface, such as the (001) $\Sigma 29$ grain boundary the DMM may be a good model for the scattering, particularly at high frequencies.

Finally, we mention that the results of this approach can be used to develop more realistic models of interfacial scattering for use in mesoscale simulation approaches. In a mesoscale approach, the energy is transported by particles localized in real space meant to represent localized phonon wave packets [9]. To describe transport in a system with interfaces, rules are required to describe the scattering at interfaces. From the results presented in this paper, one could develop a simple yet general model to describe grain boundary scattering. Specifically, our results indicate that any model should have a transmission coefficient essentially equal to unity for long-wavelength phonons. The scattering in such a model should increase with increasing frequency, with the degree of scattering gradually approaching the DMM limit at least in the case of disordered grain boundaries. Such a model would represent an improvement over current approaches that are limited either to the extremes of the AMM or the DMM.

References

1. P. L. KAPITZA, *J. Phys. (USSR)* **4** (1941) 181.
2. E. T. SWARTZ and R. O. POHL, *Rev. Mod. Phys.* **61** (1989) 605.
3. P. K. SCHELLING, S. R. PHILLPOT and K. KEBLINSKI, *Phys. Rev. B* **65**(2002) 144306.
4. *Idem.*, *J. Appl. Phys.* **95** (2004) 6082.
5. P. K. SCHELLING and S. R. PHILLPOT, *J. Amer. Ceram. Soci.* **84** (2001) 2997.
6. F. H. STILLINGER and T. A. WEBER, *Phys. Rev. B* **31** (1985) 5262.
7. A. MAITI, G. D. MAHAN and S. T. PANTELIDES, *Solid State Commun.* **102** (1997) 517.
8. P. K. SCHELLING, S. R. PHILLPOT and P. KEBLINSKI, *Appl. Phys. Lett.* **80** (2002) 2484.
9. S. MAZUMDER and A. MAJUMDAR, *J. Heat. Trans.* **123** (2001) 749.

Received 23 October 2004
and accepted 31 January 2005